CSIRO
AUSTRALIA

The CSIRO Dual-frequency Microwave Radiometer

R.H. Hill and A.B. Long

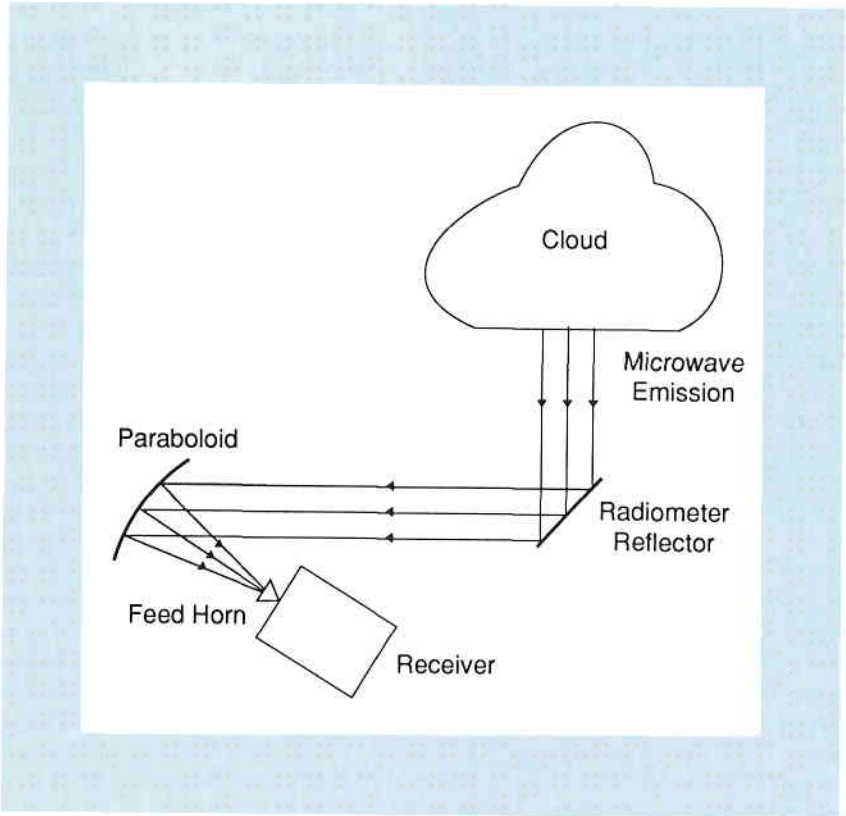

CSIRO Division of Atmospheric Research Technical Paper No. 35

THE CSIRO DUAL-FREQUENCY MICROWAVE RADIOMETER

Ronald H. Hill and Alexis B. Long
CSIRO Division of Atmospheric Research
Private Bag No. 1, Mordialloc, Vic. 3195, Australia

ABSTRACT

A dual frequency microwave radiometer is described that is used for integrated measurements of liquid water and water vapour. It operates on frequencies of 31.65 and 20.6 GHz and uses the basic design developed at NOAA Environmental Research Laboratories Environmental Technology Laboratory. Radiative transfer theory is presented and developed into the method for retrieving liquid water and vapour depths. Brightness temperature measurement and calibration are described. An example is given of the instrument in use in a cloud seeding project. Technical details of the radiometer are briefly covered.

1. Introduction

Precipitation enhancement or cloud seeding research has returned in recent years to basic atmospheric science. Of particular interest has been the amount and spatial and temporal distributions of supercooled liquid water. This liquid water is largely the source of the extra precipitation that cloud seeding attempts to produce. Improved knowledge of the supercooled liquid water will aid decisions on where and when to seed for the optimum effect.

Until recently, supercooled liquid water was assumed to exist in clouds with temperatures in the range 0°C to -15°C. An indicator of supercooled liquid water is the growth of ice from water accreting on the air frame of a seeding aircraft. A better indicator is the actual measurement of supercooled liquid water within cloud made automatically over the entire seeding time period. Such measurements have been made using a hot wire mounted on a seeding aircraft as in the Tasmania II precipitation enhancement project and elsewhere (King et al.1978, 1981, 1985; Bradley and King, 1979; King and Handsworth, 1979; Shaw et al. 1984; Biter et al. 1987).

Alternative supercooled liquid water measurements are now being made with a robust ground based microwave radiometer directed at the clouds that might be seeded. The major group involved in this development, in the 1970s and early 1980s, was the NOAA Environmental Research Laboratories Wave Propagation Laboratory, now Environmental Technology Laboratory (ETL), in Boulder, Colorado, USA. This group has published extensively on the radiometer technology, e.g. Decker et al. 1978; Guiraud et al. 1979; Hogg et al. 1983; Westwater, 1978; Westwater and Guiraud, 1980 and Westwater et al. 1988 and 1990).

In July-August 1988, the CSIRO Division of Atmospheric Research (DAR) conducted the Australian Winter Storms Experiment (AWSE) in the vicinity of Baw Baw Plateau 120 km east of

Melbourne. An objective of AWSE was to develop a field experimental understanding of how supercooled liquid water forms over and near the Plateau when a synoptic-scale winter storm is approaching the Great Dividing Range (usually from the southwest). A microwave radiometer was successfully used in the 1988 study. It was similar to the ETL model and was owned and operated by the Desert Research Institute of Reno, Nevada, USA.

On the basis of the 1988 AWSE experiment a decision was made by DAR to construct its own radiometer, with Melbourne and Metropolitan Board of Works (MMBW) financial support. (The MMBW is now known as Yarra Valley Water. The intention was that the radiometer would be operated manually, and by remote control if necessary, to detect and measure supercooled liquid water in the winter storm clouds over the Plateau. The information gained would be passed onto the MW cloud seeding group for use in deciding where and when to seed.

2. Microwave Radiometric Liquid Water Measurement

At microwave wavelengths both liquid water and water vapour absorb and emit energy. The microwave radiometer is a passive instrument that detects natural radiation emitted by cloud drops and water vapour. The emissions are detected by a microwave receiver. The received signals are processed to retrieve columnar integrated amounts of liquid water and water vapour. The dual channel radiometer is steerable to determine liquid water and water vapour in different parts of a cloud.

Hill (1991) and Snider and Hogg (1981) used single channel radiometers, which did not retrieve water vapour. A dual channel radiometric method of measurement was therefore chosen using the same basic design as Hogg et al. (1983) which retrieved both liquid water and water vapour. It uses channel frequencies of 31.5 GHz and 20.6 GHz. The 31.65 GHz channel is more sensitive to liquid water and the 20.6 GHz channel is more sensitive to water vapour. Both channels are needed for the simultaneous measurement of liquid water and water vapour in clouds. 20.6 GHz is close to the absorption line of water vapour at 22.2 GHz. The measurement would normally be expected to be made at the absorption line frequency, however absorption at this frequency varies with both the temperature and pressure of the volume of air within the antenna beam. Westwater (1978) has shown that the effect of these atmospheric variables is a minimum at 20.6 GHz.

3. The Measurement Concept

The measurement concept is shown in Figure 1. Microwave emission from liquid water and water vapour in clear air and clouds is reflected from a disk to a paraboloid, focussed into a feed horn and fed into a receiver. The receiver splits the signal into the two frequencies of 31.65 and 20.6 GHz. The signals are then amplified, detected, digitized and processed in a computer. Reference temperature loads are switched into the input waveguides of each channel. Each channel input cycles between constant temperature loads of 45°C and 145°C and the input from the feedhorn, and is therefore automatically calibrated. A more detailed description is found in Hogg et al. (1983).

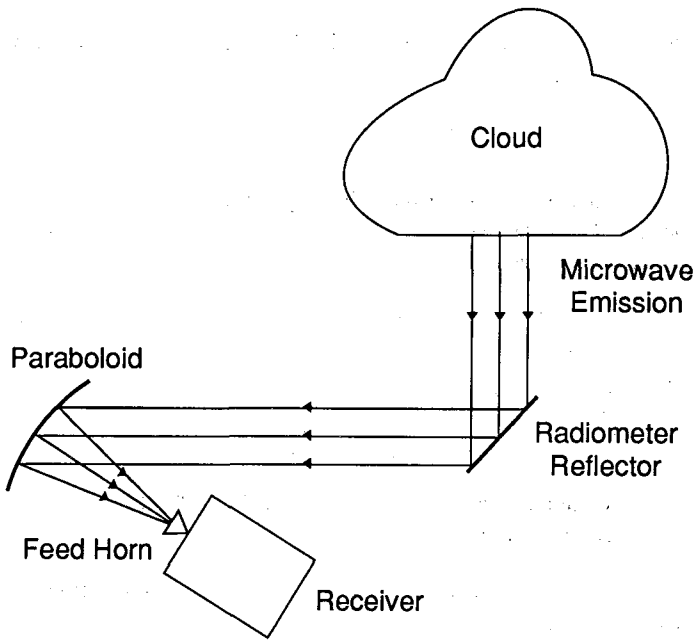

Figure 1. The microwave radiometric measurement concept.

The computer controls the antenna, computes calibration coefficients and retrieves vapour and liquid water depths. Depth can be defined as the conversion of measured integrated liquid and vapour into uniform layers in the atmosphere of equivalent depths.

4. Atmospheric Radiative Transfer

The equation of radiative transfer from the zenith direction has the form (Wei et al. 1989),

$$I(z=o) = I_e\, t(o,\infty) + \int_o^\infty B(z)\gamma(z)\, t(o,z)\, dz \qquad (1)$$

where $I(z=o)$ is the monochromatic radiance viewed from the ground surface ($z=o$), I_e is the extraterrestrial radiance, $t(o,\infty)$ is the transmittance from infinite distance to the surface, $B(z)$ is the Planck spectral radiance from within the atmosphere, and $\gamma(z)$ is the volume absorption coefficient. The transmittance $t(o,z)$ is related to the total optical thickness $\tau(o,z)$ by:

$$t(o,z) = \exp\,[-\tau(o,z)] \qquad (2)$$

The total optical thickness in turn is related to the total volume absorption coefficient γ of all species by:

$$\tau(o,z)=\int_o^z \gamma(y)dy \tag{3}$$

The quantities in (1) are spectral, having values that depend on the wavelength (λ) of radiation. The formulation above of the radiative transfer equation is valid for clear or cloudy skies but not for skies with heavy rain or melting snow in which scattering would not be negligible.

The Planck function in (1) can be approximated by the Rayleigh-Jeans radiation law when $hc/k\lambda T$ is small. The approximation for the spectral radiance $B(z)$, from Goody (1964), is the following:

$$\frac{2\pi\, ckT(z)}{\lambda^4} \approx B(z)=\frac{2\pi\, c^2 h}{\lambda^5}\frac{1}{[\exp[hc\,/\,k\lambda T(z)]-1]} \tag{4}$$

(Rayleigh-Jeans approximation) (Planck function)

where h is Planck's constant, $T(z)$ is the atmospheric temperature profile, k is Boltzmann's constant and c is the microwave frequency.

The left-hand expression above is substituted for the blackbody radiance $B(z)$ in the right-hand side of equation (1). Additionally, it is assumed that the other radiances in equation (1) are equivalent to emissions from blackbodies of designated brightness temperatures. The result of the substitutions is:

$$T_B(z=o)=T_{Be}\, t(o,\infty)+\int_o^\infty T(z)\gamma(z)t(o,z)dz \tag{5}$$

where T_B is the downwelling blackbody brightness temperature at the surface measured with the radiometer, T_{Be} (= 2.75K) is the brightness temperature of the extraterrestrial radiance.

Differentiating (2) and (3) with respect to z and eliminating $\partial\tau/\partial z$ between them yields:

$$\frac{\partial t}{\partial z}=-\gamma(z)t(o,z) \tag{6}$$

Substituting (6) into (5) yields

$$T_B(z=o)=T_{Be}\, t(o,\infty)+\int_o^\infty T(z)\left(\frac{-\partial t}{\partial z}\right)dz \tag{7}$$

Let T_m, the mean radiating temperature of the atmosphere at the experimental site, be introduced into equation (7) such that:

$$T_B(z=o)=T_{Be}\, t(o,\infty)+T_m\int_o^\infty \frac{-\partial t}{\partial z}dz \tag{8}$$

Therefore

$$T_B = T_{Be}\, t(o,\infty) + T_m\, [1 - t(o,\infty)] \tag{9}$$

and

$$t(o,\infty) = (T_m - T_B) / (T_m - T_{Be}) \tag{10}$$

thus

$$\tau(o,\infty) = -ln[(T_m - T_B) / (T_m - T_{Be})] \tag{11}$$

5. Variable Retrieval

The optical depths in (11) are used to obtain the water vapour and liquid water depth at each of the two microwave operating frequencies.

The optical depth due to water vapour is:

$$\tau_V = \int_o^\infty \rho_V\, k_V\, dz = K_V\, V \tag{12}$$

where ρ_V is the water vapour density, k_V is the mass absorption coefficient of water vapour, K_V is the water vapour density-weighted vertical mean mass absorption coefficient and V is the vertical integrated total columnar vapour or precipitable water. Similarly:

$$\tau_L = \int_o^\infty M k_L\, dz = K_L L \tag{13}$$

where τ_L is the optical thickness of liquid water, M is the mass of liquid water per unit volume of air, k_L is the mass absorption coefficient of liquid water, K_L is the weighted vertical mean mass absorption coefficient and L is the vertical integrated total columnar liquid water depth.

Oxygen is also radiative. Its optical thickness is calculated from

$$\tau_0 = \int_o^\infty m_0 \rho\, k_0\, dz \tag{14}$$

where m_0 is the mixing ratio of oxygen, ρ is the air density and k_0 the mass absorption coefficient of oxygen.
Total optical thickness τ is calculated from

$$\tau = \tau_V + \tau_L + \tau_0 \tag{15}$$

Equations (12), (13), (14) and (15) can be used to determine the precipitable water vapour depth V and liquid water depth L.

The relevant equations to be solved for V and L are:

$$K_{V1} V + K_{L1} L + \tau_{01} = \tau_1 \quad (16a)$$
$$K_{V2} V + K_{L2} L + \tau_{02} = \tau_2 \quad (16b)$$

where 1 and 2 refer to frequencies 20.6 GHz and 31.65 Ghz respectively.

They yield:

$$L = \frac{K_{V2}(\tau_1 - \tau_{01}) - K_{V1}(\tau_2 - \tau_{02})}{K_{V2}K_{L1} - K_{V1}K_{L2}} \quad (17a)$$

$$V = \frac{K_{L2}(\tau_1 - \tau_{01}) - K_{L1}(\tau_2 - \tau_{02})}{K_{L2}K_{V1} - K_{L1}K_{V2}} \quad (17b)$$

which, following Wei et al., readily simplify to:

$$L = A_0 + A_1 \tau_1 + A_2 \tau_2 \quad (18a)$$
$$V = B_0 + B_1 \tau_1 + B_2 \tau_2 \quad (18b)$$

where:

$$A_0 = (-K_{V2} \tau_{01} + K_{V1} \tau_{02})/D$$
$$A_1 = K_{V2}/D$$
$$A_2 = -K_{V1}/D$$
$$B_0 = (-K_{L1} \tau_{02} + K_{L2} \tau_{01})/D$$
$$B_1 = -K_{L2}/D$$
$$B_2 = K_{L1}/D$$

and:

$$D = K_{V2} K_{L1} - K_{V1} K_{L2}.$$

Solution of (18a) and (18b) requires knowing both the atmospheric climatological parameters A_i, B_i, and the parameters and variables composing τ_i. The subscript $i = 1,2$ denotes one of the two radiometer operating frequencies, 20.6 GHz and 31.65 GHz. A_i and B_i depend on the parameter K_{Vi}, K_{Li} and τ_{Oi}. Climatological averages of each of these parameters are calculated using radiosonde measurements collected in the space-time vicinity of the radiometer measurements.

The optical depths τ_i are evaluated from (11). The variables T_{Bi} are brightness temperatures determined from radiometer measurements in the two frequency channels. Later Sections of this paper discuss the measurement and calibration of T_{Bi}. The variable T_{Be} is the temperature (= 2.75 K) of the cosmic extraterrestrial blackbody radiance at the Earth's surface. T_{mi} is the mean

radiating temperature of the atmosphere. Using equations 5 and 9, T_{mi} is defined as:

$$T_{mi} = \int_{o}^{\infty} T(z)\gamma(z)t(o,z)dz \,/\, (1 - t(o,\infty)) \tag{19}$$

From radiosonde data on the temperature profile $T(z)$ and information from the volume absorption coefficient profile $\gamma_i(z)$ the integrals and, hence, T_{mi} can be calculated.

Once all of the parameters A_i, B_i and measurables τ_i are in hand the next step is to use (17a) and (17b) to calculate the integrated depths of liquid water L and water vapour V.

6. Brightness Temperature Measurement

The brightness temperatures T_{B1} and T_{B2} used in determining τ_1 and τ_2 are calculated from (20) using temperatures and voltages measured inside the radiometer. An extended treatment of the calculations appears in Decker and Schroeder (1991). In this equation

$$T_{Bi} = (CF_o)(XL_o)\left[\left(\frac{VDM - VDR_o}{VAH - VAR_o}\right)\left(\frac{VAH_o - VAR_o}{VDH_o - VDR_o}\right)(TH - TR)\right] + (XL_o)(TR - TW) + TW \tag{20}$$

T_B represents brightness temperature, i the radiometer microwave frequency used (i = 1,2), CF_o is a calibration constant, XL_o is a loss factor, VDM is the continuously monitored data channel voltage, VDR_o and VDH_o are reference offset voltages measured in the data channel, VAH_o and VAR_o are reference offset voltages measured in the Automatic Gain Control (AGC) channel. The reference offset voltages are measured on an hourly basis. VAH is a continuously monitored voltage in the AGC channel. TH and TR are the hot load and reference load temperatures. TW is the input waveguide temperature.

The AGC channel is used to monitor changes in gain and offset that occur during operation, and is used as an automatic gain control for the measurement channel.

7. Brightness Temperature Calibration

The temperatures T_{Bi} must be calibrated before they are used to obtain vapour and liquid. Decker and Schroeder (1991) describe two methods of calibration, the *radiosonde calibration method* and the *tipping curve calibration method.*

Radiosonde calibration method

Radiometer brightness temperatures and brightness temperatures from radiosonde pressure, temperature and humidity data are compared over a period of time such as a month. Brightness temperatures calculated from radiosonde profiles are taken as the true values that the radiometer should reproduce. Only clear conditions are used. The radiosonde data of temperature, pressure

and humidity are used to evaluate the radiative transfer equation, equation (21), which was derived from equations (2), (3) and (5).

$$T_{Bn} = T_{Be} \exp\left[-\int_o^\infty \gamma(y)dy\right] + \int_o^\infty T(z)\gamma(z)\exp\left[-\int_o^z \gamma(y)dy\right]dz \qquad (21)$$

T_{Bn} is the new true brightness temperature. The volume absorption coefficient γ at height y in (21) is calculated from the atmospheric absorption model of Liebe and Layton(1987) with interference coefficients from Rosenkranz (1988).

When initial radiometric measurements are made, calibration factors CF_o and XL_o have assumed values. The measured brightness temperature, T_{Bo}, is calculated from equation (20) using these assumed values. Once the true brightness temperature, T_{Bn}, is known from (21), it is then required to find the calibration factors CF_n and XL_n that will minimise the difference between T_{Bn} and T_{Bo}.

Equation 20 is first written using the values T_{Bo}, CF_o and XL_o. It is then rewritten using values T_{Bn}, CF_n and XL_n, as in (22) below.

$$T_{Bn} = (CF_n)(XL_n)\left[\left(\frac{VDM - VDR_O}{VAH - VAR_O}\right)\left(\frac{VAH_O - VAR_O}{VDH_O - VDR_O}\right)(TH - TR)\right] + (XL_n)(TR - TW) + TW \qquad (22)$$

Each equation can then be transposed to leave the term

$$\left[\left(\frac{VDM - VDR_o}{VAH - VAR_o}\right)\left(\frac{VAH_o - VAR_o}{VDH_o - VDR_o}\right)(TH - TR)\right]$$

on the right hand side. As this term is common to both equations, the left hand side terms may be equated as below

$$\frac{T_{Bo} - XL_o(TR - TW) - TW}{(CF_o)(XL_o)} = \frac{T_{Bn} - XL_n(TR - TW) - TW}{(CF_n)(XL_n)} \qquad (23)$$

from which:

$$\left[\frac{T_{Bo} - XL_o(TR - TW) - TW}{(CF_o)(XL_o)}\right](CF_n)(XL_n) + (TR - TW)XL_n + (TW - T_{Bn}) = 0 \qquad (24)$$

The square bracketed term in (24) can be evaluated from the radiometer. The terms CF_o, and XL_o are original radiometer calibration factors. The unknown calibration factors CF_n and XL_n can be obtained from the above equation by treating it as an expression to be minimised in the least squares sense.

The expression is:

$$\sum_{i=1}^{m}(a_i\,x+b_i\,w+c_i)^2 \tag{25}$$

with
a_i = square bracketed term in (24)
b_i = TR-TW
c_i = TW-T_{Bn}
x = $(CF_n)(XL_n)$
w = Xl_n .

The number m of radiosonde data sets, and of matching radiometer data sets, may have to be large in order for meaningful solutions for x and w to be obtained.

Tipping curve calibration method

The tipping curve calibration method requires making radiometer brightness temperature measurements at several different elevation angles of the radiometer under clear atmospheric conditions. Each elevation angle represents a different air mass. When the measurement is made toward the zenith, the air mass is considered equal to one. The air mass is approximately equal to the cosecant of the elevation angle. Total absorption is linear with air mass. The relationship between total absorption and brightness temperature is shown in equation (11).

A plot of total absorption against air mass must pass through the origin, as absorption at zero air mass must be zero. If the plot does not pass through the origin then brightness temperatures are not true, and the absorption is not true. The entire plot of absorption against air mass is then offset so as to pass through the origin. This then gives true absorption τ_n. True brightness temperature T_{Bn} can then be calculated from (11) transposed to solve for T_{Bn}.

Using true brightness temperatures, new calibration coefficients can be calculated. If XL in (23) is chosen from engineering considerations and is assumed not to vary then $XL_n = XL_o = XL$. Substituting these into (23) and solving for CF_n, the equation becomes:

$$CF_n = \left(\frac{T_{Bn} - XL(TR-TW) - TW}{T_{Bo} - XL(TR-TW) - TW}\right) CF_o \tag{26}$$

where CF_n is the new calibration coefficient.

The tipping curve calibration method is used more frequently because of its relative simplicity.

8. Liquid Water Radiometer Description

A schematic diagram of the instrument is shown in figure 2. It is built to fit on the back of a four-tonne truck, but is removable to enable transport by air or sea.

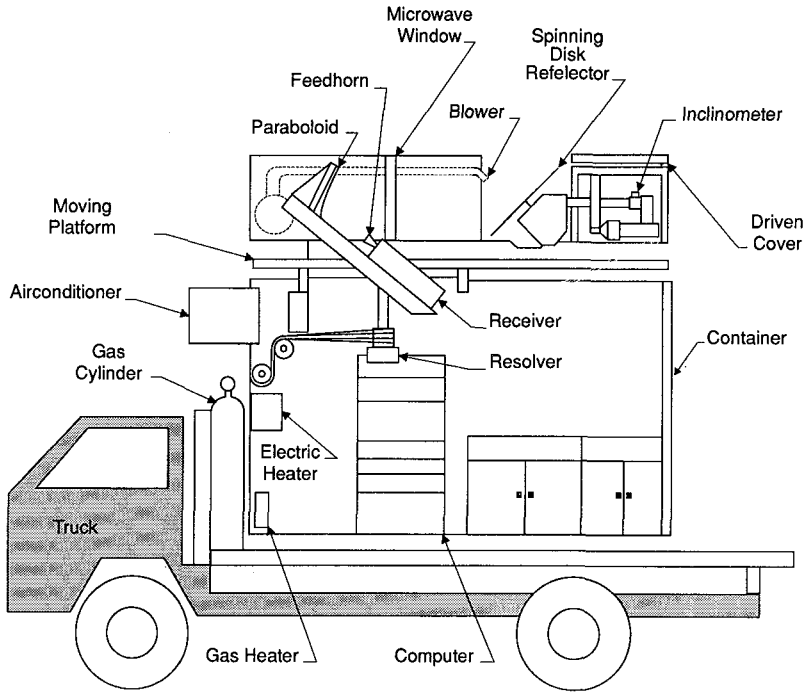

Figure 2. A schematic diagram of the Liquid Water Radiometer.

The incoming cloud and sky radiation is reflected from the spinning disk to the offset paraboloid onto the feedhorn of the dual channel microwave radiometer receiver, as shown in figure 1. The radiometer receiver was built by Hughes Aircraft Company to the specifications of the ETL. It is of the Dicke switching type as described in Guiraud et al. (1979). A detailed functional schematic diagram is shown in Hogg et al. (1983). Essentially there are two radiometer receivers in the package, one operating at 31.65 GHz and the other at 20.6 GHz. Both receive radiation through a single feedhorn. The feedhorn is a corrugated, multi-mode design similar to that described in Hogg et al. (1979). The antenna system acceptance angle for the received radiation is 2.5°.

The radiometer receiver is seated in a motor driven antenna structure mounted on a one metre diameter slew bearing. The slew bearing provides almost 360° of rotation in azimuth. It is driven by a stepping motor controlled by a computer through an indexer. The offset paraboloid, microwave window, blower, spinning disk and spinning disk drive, cover and cover drive are also mounted on the antenna. Antenna position (azimuth) is sensed by a resolver and can be selected to within 0.1 degrees of rotation.

Inside and outside air are separated in the signal path by an eccofoam microwave window, mounted between sheets of mylar film. This window is housed well out of the weather so as to minimise snow and rain wetting the surface. A wet surface causes errors in absorption readings. Snow and rain also cause errors when on the surface of the reflecting disk. Spinning the disk causes snow and water to be thrown off by centrifugal force. Centrifugal force is weak near the centre of the disk and a blower is directed to the centre to blow the snow and water away from there.

The instrument was intended to be switched on and off remotely. It was important therefore to prevent a build-up of snow and ice on the disk during off periods. For this purpose a motor drives a cover over the spinning disk just prior to shutdown. The spinning disk would normally be directed toward the zenith. However it can be driven toward the horizontal so as to face either east or west. Switches limit travel to about ±80°. Elevation is sensed with an inclinometer. The spinning disk assembly is also driven by a stepping motor computer controlled through an indexer.

Within the housing, temperature is controlled by a heater-controller for heating and an air conditioner for cooling. The controller switches both the heater and air conditioner. It maintains the internal temperature to within 0.1°C. An additional fan has been added to ensure the air in the cavity above the slew ring is properly mixed. A liquid petroleum gas heater is used to maintain the air above condensation temperature when the instrument is not in use. It is set to maintain air at about 10°C.

The instrument was designed to be powered remotely by a generator. The generator is a 10 kW Lister-Peter machine. The generator must start up as part of the remote switch-on process. For remote switch on, a low power DC modem is used in conjunction with a low power single board computer, that has a standby mode. When the carrier is detected by the modem the circuitry is turned on to full power and a relay is activated that switches the generator on. Switch off is initiated by a software command.

The computer is a semi-industrial AT with a 386 microprocessor made by Qualogy. Burr-Brown analogue to digital, digital to analogue and interface boards are used.

The software was developed by a private contractor: Adacel Pty. Ltd. A real time multi-tasking operating system was needed and QNX was selected. The software developed requires about 2 megabytes of memory. Data are stored on a large rolling file. That is, once the file is full, incoming data overwrite the oldest record in the file. The data are recorded and transmitted in records of 141 bytes length. These include time and date, flags, atmospheric variables, radiometer variables and reference parameters, all important voltages and temperatures that will enable fault diagnosis. Data were transmitted down the remote control data link at 2400 baud using an error checking protocol. Control needed to be maintained from the remote end. If there was a long period of noise on the line, or if there was a significant loss of carrier then the software was designed to shut down the instrument.

The software is designed into scans and schedules. Schedules time the operation of the radiometer. Scans control it's operation. The scans may be selected to be constant position, constant elevation, constant azimuth, sector and tipping curve. The sector passes in turn through fixed azimuth and elevation segments. The tipping curve scan allows five angles of elevation to be selected and the scanning is performed for each of these angles in turn.

A photograph of the instrument is shown in figure 3.

Figure 3. A photograph of the instrument in operation on Mount Baw Baw.

9. Cloud Seedability from Radiometer & Precipitation Data

The dual-frequency microwave radiometer can be used along with precipitation data to estimate cloud seedability, or the potential increase in precipitation from cloud seeding. An example of this data use is provided here for a precipitating weather system. Figure 4 shows the liquid water recorded by the radiometer for a sixteen-hour period on 8 August 1992.

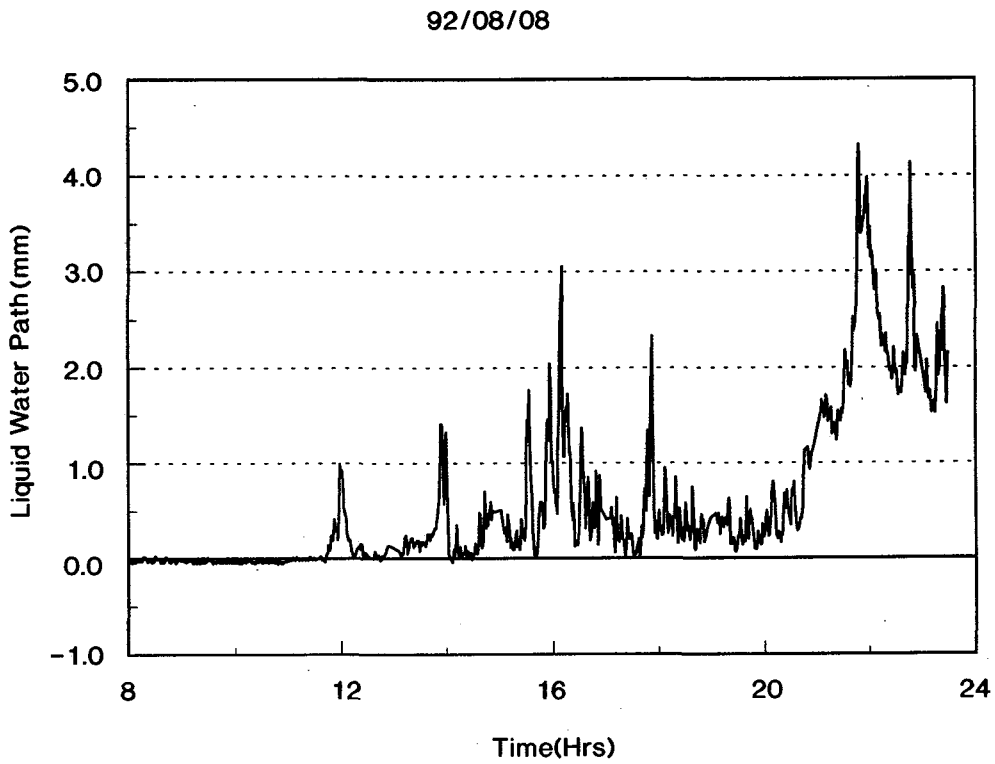

Figure 4. Liquid water measured by the radiometer on 8 August, 1992.

Synoptic, surface weather maps have been obtained at three-hour intervals for the period 2100 Eastern Standard Time (EST) 7 August 1992 to 2100 EST 8 August 1992. The maps show a cold front, orientated north-south, passing across the Baw Baw Plateau study area east of Melbourne where the radiometer was located. The time of frontal passage was between 1500 and 1800 on 8 August. Just prior to frontal passage, at 1200, a surface low of about 1002 hPa had formed along the front in northern Victoria and southern New South Wales.

Near the times of the frontal passage and surface low formation, 1 mm of precipitation was observed to fall in 30-minute periods, respectively, in the tipping bucket precipitation gauge on Baw Baw Plateau. After the front had passed, an enhanced precipitation rate was observed. From 2030 to 2300 a total of 5.6 mm fell, at a mean rate of 2.2 mm hr^{-1}. The maximum rate was 3.6 mm hr^{-1} in the 30-minute period from 2130-2200.

Radiometer data on the vertical line integral (depth) of liquid water (mm) were collected throughout this period. The second column in Table 1 shows the depths that were measured. The third column shows the corresponding precipitation rates.

Column four shows the ratio of column two to column three. This ratio W/r is the minimum time T_a for complete consumption of supercooled liquid water. The time will be longer if ice processes are contributing to the precipitation rate. A useful quantity for normalising T_a is the kinematic time T_b required for the in-cloud supercooled liquid water to move across a target area over which cloud seeding is to increase precipitation. The ratio of $T_a/T_b = \sigma$, the seedability, is the time needed to consume by precipitation the supercooled liquid water over the target area divided by the

precipitation time available over the target area. A typical value for T_b for the Melbourne Water target area is about 0.5 hr. Thus the seedability was a minimum of 1.0-5.0 for this storm. The potential increase in precipitation by cloud seeding took on larger values later in the storm. The seedability then was high.

It is clear that the main variables influencing the seedability are the supercooled liquid water depth (measured with the radiometer) and the precipitation rate (measured by the rain gauges). Use of real-time information from these instruments can greatly assist cloud seeders in determining when to seed clouds.

Table 1. Comparison of radiometer integrated liquid water depth and gauge precipitation amount and their ratio

Time (EST) 8 August 1992	***W*** **Liquid water depth (mm)**	***r*** **Precipitation rate (mm hr^{-1})**	$T_a = W/r$ **(hr)**	σ = **Seedability**
1200-1230	1.0	2.0	0.5	1.0
1400-1430	1.4	2.0	0.7	1.4
2000-2030	0.4	0.8	0.5	1.0
2030-2100	0.8	1.6	0.5	1.0
2100-2130	1.4	2.4	0.6	1.2
2130-2200	2.7	3.6	0.8	1.6
2200-2230	2.5	1.6	1.6	3.2
2230-2300	2.0	2.0	1.0	2.0
2300-2330	2.0	0.8	2.5	5.0

10. Acknowledgments

We acknowledge the financial assistance of Melbourne Water, which made the radiometer possible. We are grateful for the technological help of Jack Snider and Ed Westwater of the NOAA Environmental Technology Laboratory and Dick Smith of the Desert Research Institute. Also, Helen Dickinson of Adacel Pty. Ltd. for the software and Bill Layton of Austek Pty. Ltd. for most of the mechanical design. We are thankful for the efforts of all the staff of the CSIRO Division of Atmospheric Research who participated in the manufacture of the radiometer. These include John Bennett, Patrick Bradley, Deryk Hartwick, Reg Henry, Rick McDonald, Peter Nelson, Bernard Petraitis, Craig Phelan, Craig Smith, Laurie Tout, Brian Turner and Chris Walley.

References

Bradley, S.G., and W.D. King (1979). Frequency response of the CSIRO liquid water probe. *J. Appl. Meteor.*, **18,** 361–366.

Biter, C.J., J.E. Dye, D. Huffman and W.D. King (1987). The drop-size response of the CSIRO liquid water probe. *J. Atmos. Oceanic Tech.*, **4**, 359–367.

Decker, M.T., E.R. Westwater and F.O. Guiraud (1978). Experimental evaluation of groundbased microwave radiometric sensing of atmospheric temperature and water vapour profiles.

Decker, M.T., and J.A. Schroeder (1991). Calibration of groundbased microwave radiometers for atmospheric remote sensing. NOAA Technical Memorandum ERL WPL-197. NOAA Wave Propagation Laboratory, Boulder, 16pp.

Goody, R.M. (1964). Atmospheric Radiation. Clarendon Press at Oxford, 30–31.

Guiraud, F.O., J. Howard and D.C. Hogg (1979). A dual-channel microwave radiometer for measurement of precipitable water vapour and liquid. *IEEE Trans. Geosci. Elec.*, **GE-17**, 129–136.

Hill, G.E. (1991). Measurement of atmospheric liquid water by a ground based single frequency microwave radiometer. *J. Atmos. Oceanic. Tech.*, **8**, 685–690.

Hogg, D.C., F.O. Guiraud, J. Howard, A.C. Newell, D.P. Kremer and A.G. Repjar (1979). An antenna for dual-wavelength radiometry at 21 and 32 GHz. *IEEE Trans. Antennas Propg.*, **AP-27**, 764–771.

Hogg, D.C., F.O. Guiraud, J.B. Snider, M.T. Decker and E.R. Westwater (1983). A steerable dual-channel microwave radiometer for measurement of water vapour and liquid in the troposphere. *J. Clim. Appl. Meteor.*, **22**, 789–806.

King, W.D., D.A. Parkin and R.J. Handsworth (1978). A hot-wire liquid water device having fully calculable response characteristics. *J. Appl. Meteor.*, **17**, 1809–1813.

King, W.D. and R.J. Handsworth (1979). Total droplet concentrations and average droplet sizes from simultaneous liquid water content and extinction measurements. *J. Appl. Meteor.*, **18**, 940–944.

King, W.D., C.T. Maher and G.A. Hepburn (1981). Further performance tests on the CSIRO liquid water probe. *J. Appl. Meteor.*, **20**, 195–202.

King, W.D., J.E. Dye, J.W. Strapp, D. Baumgardner and D. Huffman (1985). Icing wind tunnel tests on the CSIRO liquid water probe. *J. Atmos. Oceanic Tech.*, **2**, 340–352.

Liebe, H.J. and D.H. Layton (1987). Millimetre-wave properties of the atmosphere : Laboratory studies and propagation modelling, NTIA Report 87-224, National Telecommunications and Information Administration, Boulder, CO, 74pp.

Rosenkranz, P.W. (1988). Interference coefficients for overlapping oxygen lines in air, *J. Quant, Spectros. Radiat. Transfer*, **39**, 287–297.

Shaw, D.E., W.D. King, and E. Turton (1984). Analysis of Hydro-Electric Commission cloud seeding in Tasmania, 1979-1983. CSIRO Division of Cloud Physics Report CP394. Division of Cloud Physics, Epping, 70pp.

Snider, J.B., and D.C. Hogg (1981). Ground-based radiometric observations of cloud liquid in the Sierra Nevada. NOAA Technical Memorandum ERL WPL-72.

Wei, C., H.G. Leighton and R.R. Rogers (1989). A comparison of several radiometric methods of deducing path-integrated cloud liquid water. *J. Atmos. Oceanic Tech.*, **6**, 1001–1012.

Westwater, E.R. (1978). The accuracy of water vapour and cloud liquid determination by dual frequency groundbased microwave radiometry. *Radio Science*, **13**, 677–685.

Westwater, E.R. and F.O. Guiraud (1980). Ground-based microwave radiometric retrieval of precipitable water vapour in the presence of clouds with high liquid content. *Radio Science*, **15**, 947–957.

Westwater, E.R., J.B. Snider and M. Falls (1988). Observations of atmospheric emission and attenuation at 20.6, 31.65 and 90 GHz by a ground-based radiometer. NOAA Technical Memorandum ERL WPL-156. NOAA Wave Propagation Laboratory, Boulder, 16pp.

Westwater, E.R., J.B. Snider and M.J. Falls (1990). Ground based radiometric observations of atmospheric emission and attenuation at 20.6, 31.65 and 90.0 GHz: A comparison of measurements and theory. *IEEE Trans. Ant. Prop.*, **38**, 1569–1580.

CSIRO DIVISION OF ATMOSPHERIC RESEARCH TECHNICAL PAPERS

No. 1 Galbally, I.E., Roy, C.R., O'Brien, R.S., Ridley, B.A., Hastie, D.R., Evans, W.J.F., McElroy, C.T., Kerr, J.B., Hyson, P., Knight, W. & Laby, J.E., *Measurements of Trace Composition of the Austal Stratosphere*: chemical and meteorological data, 1983. p. 31.

No. 2 Enting, I.G., *Error Analysis for Parameter Estimates from Constrained Inversion*, 1983, p. 18.

No. 3 Enting, I.G. & Pearman, G.I., *Refinements to a One-Dimensional Carbon Cycle Model*, 1983, p. 35.

No. 4 Francey, R.J., Barbetti, M., Bird, T., Beardsmore, D., Coupland, W., Dolezal, J.E., Farquhar, G.D., Flynn, R.G., Fraser, P.J., Gifford, R.M., Goodman, H.S., Kunda, B., McPhail, S., Nanson, G., Pearman, G.I., Richards, N.G., Sharkey, T.D., Temple, R.B. & Weir, B., *Isotopes in Tree Rings*, 1984, p. 86.

No. 5 Enting, I.G., *Techniques for Determining Surface Sources from Surface Observations of Atmospheric Constituents*, 1984, p. 30.

No. 6 Beardsmore, D.J., Pearman, G.I. & O'Brien, R.C., *The CSIRO (Australia) Atmospheric Carbon Dioxide Monitoring Program:* surface data, 1984, p. 115.

No. 7 Scott, J.C. *High Speed Magnetic Tape Interface for a Microcomputer,* 1984, p. 17.

No. 8 Galbally, I.E., Roy, C.R., Elsworth, C.M. & Rabich, H.A.H., *The Measurement of Nitrogen Oxide (NO, NO_2) Exchange over Plant/Soil Surfaces*, 1985, p. 23.

No. 9 Enting, I.G., *A Strategy for Calibrating Atmospheric Transport Models*, 1985, p. 25.

No. 10 O'Brien, D.M., TOVPIX: *Software for Extraction and Calibration of TOVS Data from the High Resolution Picture Transmission from TIROS-N Satellites*, 1985, p. 41.

No. 11 Enting, I G. & Mansbridge, J.V., *Description of a Two-Dimensional Atmospheric Transport Model*, 1986, p. 22.

No. 12 Everett, J.R., O'Brien, D.M. & Davis, T.J., *A Report on Experiments to Measure Average Fibre Diameters by Optical Fourier Analysis,* 1986, p. 22.

No. 13 Enting, I.G., *A Signal Processing Approach to Analysing Background Atmospheric Constituent Data,* 1986, p. 21.

No. 14 Enting, I.G. & Mansbridge, J.V., *Preliminary Studies with a Two–Dimensional Model Using Transport Fields Derived from a GCM,* 1987, p. 47.

No. 15 O'Brien, D.M. & Mitchell, R.M., *Technical Assessment of the Joint CSIRO/Bureau of Meteorology Proposal for a Geostationary Imager/Sounder over the Australian Region*, 1987, p. 53.

No. 16 Galbally, I.E., Manins, P.C., Ripari, L. & Bateup, R., *A Numerical Model of the Late (Ascending) Stage of a Nuclear Fireball,* 1987, p. 89.

No. 17 Durre, A.M. & Beer, T., *Wind Information Prediction Study:* Annaburroo Meteorological Data Analysis. 1989. p. 30. + diskette.

No. 18 Mansbridge, J.V. & Enting, I.G., *Sensitivity Studies in a Two–Dimensional Atmospheric Transport Model*, 1989, p. 33.

No. 19 O'Brien, D.M. & Mitchell, R.M., Zones of Feasibility for Retrieval of Surface Pressure from Observations of Absorption in the A Band of Oxygen, 1989, p. 12.

No. 20 Evans, J.L., *Envisaged Impacts of Enhanced Greenhouse Warming on Tropical Cyclones in the Australian Region*, 1990, p. 31. (out of print)

No. 21 Whetton, P.H. & Pittock, A.B., *Australian Region Intercomparison of the Results of some General Circulation Models used in Enhanced Greenhouse Experiments*, 1991, p. 73. (out of print)

No. 22 Enting, I. G., *Calculating Future Atmospheric CO_2 Concentrations*, 1991, p. 32.

No. 23 Kowalczyk, E.A., Garratt, J.R. & Krummel, P.B., *A Soil–Canopy Scheme for use in a Numerical Model of the Atmosphere — 1D Stand–Alone Model,* 1992, p. 56.

No. 24 Physick, W.L., Noonan, J.A., McGregor, J.L., Hurley, P.J., Abbs, D.J. & Manins, P.C. *LADM: A Lagrangian Atmospheric Dispersion Model*, 1994, p. 137.

No. 25 Enting, I.G., *Constraining the Atmospheric Carbon Budget*: a preliminary assessment, 1992, p. 28.

No. 26 McGregor, J.L., Gordon, H.B., Watterson, I.G., Dix, M.R. & Rotstayn, L.D., *The CSIRO 9–Level Atmospheric General Circulation Model,* 1993, p. 89.

No. 27 Enting, I.G. & Lassey, K.R., *Projections of Future CO_2.* (Appendix by R.A. Houghton) 1993, p. 42.

No. 28 (Not published)

No. 29 Enting, I. G., Trudinger, C.M., Francey, R.J., & Granek, H., *Synthesis Inversion of Atmospheric CO_2 using the GISS Tracer Transport Model*, 1993, p. 44.

No. 30 O'Brien, D. M., *Radiation Fluxes and Cloud Amounts Predicted by the CSIRO 9–Level GCM and Observed by ERBE and ISCCP,* 1993, p. 37.

No. 31 Enting, I.G., Wigley, T.M.L. & Heimann, M., *Future Emissions and Concentrations of Carbon Dioxide*: key ocean/atmosphere/land analyses, 1994, p. 120.

No. 32 Kowalczyk, E.A. Garratt, J.R. & Krummel, P.B., *Implementation of a Soil-Canopy Scheme into the CSIRO GCM—Regional Aspects of the Model Response*, 1994, p. 59.

No. 33 Prata, A.J., *Validation Data for Land Surface Temperature Determination from Satellites*, 1994, p. 40.

No. 34 Dilley, A.C. & Elsum, C.C., *Improved AVHRR Data Navigation using Automated Land Feature Recognition to correct a Satellite Orbital Model*, 1994, p. 22.